Confinement-induced interlayer molecules: A route to strong interatomic interactions

M. Kanász-Nagy, E. A. Demler, and G. Zaránd

Confinement induced interlayer molecules: a route to strong interatomic interactions

M. Kanász-Nagy[1], E. A. Demler[2] and G. Zaránd[3]

[1]*Condensed Matter Research Group of the Hungarian Academy of Sciences, Budafoki út 8., H-1111 Budapest, Hungary*
[2]*Department of Physics, Harvard University, Cambridge, MA 02138, U.S.A and*
[3]*BME-MTA Exotic Quantum Phases Research Group,*
Budapest University of Technology and Economics, Budapest 1521, Hungary

We study theoretically the interaction between two species of ultracold atoms confined into two layers of a finite separation, and demonstrate the existence of new types of confinement-induced interlayer bound and quasi-bound molecules: these novel exciton-like interlayer molecules appear for both positive and negative scattering lengths, and exist even for layer separations many times larger than the interspecies scattering length. The lifetime of the quasi-bound molecules grows exponentially with increasing layer separation, and they can therefore be observed in simple shaking experiments, as we demonstrate through detailed many-body calculations. These quasi-bound molecules can also give rise to novel interspecies Feshbach resonances, enabling one to control geometrically the interaction between the two species by changing the layer separation. Rather counter-intuitively, the species can be made strongly interacting, by actually increasing their spatial separation. The separation induced interlayer resonances provide a powerful tool for the experimental control of interspecies interactions and enables one to realize novel quantum phases of multicomponent quantum gases.

I. INTRODUCTION

The world of low-dimensional quantum systems has attracted and continues to attract immense interest. In lower spatial dimensions, interactions and quantum fluctuations both play a determining role, and give rise to exotic quantum states such as Luttinger liquids, fractional quantum Hall [1] and quantum spin Hall states [2, 3] or various kinds of spin liquid states, not to mention the family of high temperature superconductors, where effective two-dimensionality seems to play a crucial role, too [4].

Ultracold atoms open radically new perspectives in studying low-dimensional quantum systems. Quasi-two-dimensional and one-dimensional structures can now be created with ease by means of deep optical lattices [5, 6], single 'pancake' and 'cigar-shaped' traps [7, 8] or Hermite-Gaussian laser beams [9], and their dynamical and interaction properties can be investigated systematically [5–8, 10–13]. In fact, the rapidly improving experimental control of these optical systems has gradually promoted them to 'quantum simulators' [14, 15], and allows to test the validity of various theoretical approaches systematically.

Layered two-dimensional multi-component systems provide a particularly exciting perspective within the field of ultracold atoms. Such systems should enable one to create the cold atomic analogues of interaction-driven condensed matter states such as excitonic Bose condensates [16, 17] integer and fractional quantum-Hall states [18–23] observed in bilayer two-dimensional quantum well structures. More recently a similarly rich quantum Hall behavior [24, 25] and the emergence of zero field magnetic phases have been observed in bilayer graphene [26–28]. As an even more interesting possi-
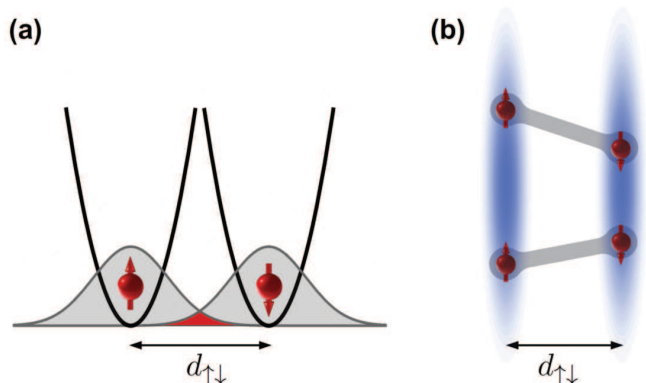

FIG. 1. (Color online.) (a) Experimental setup. A two component gas is confined into quasi-two-dimensions using an optical lattice in the z direction. The components can be separated into two layers either by using a perpendicular magnetic field gradient, or through vectorial light shifts produced by the laser field. (b) Schematic picture of the separated clouds. Quasi-bound states between atoms in different layers can lead to resonant interlayer interactions.

bility, multicomponent fermionic and bosonic systems in restricted geometries open the possibility of realizing exotic quantum states of matter [29–32], never observed before. Multicomponent bosonic superfluids are expected to exhibit a rich phase diagram of Kosterlitz–Thouless phases, and intriguing quantum phase transitions, moreover, the special structure of topological excitations in certain spinful condensates is expected to modify the character of the phase transition [33, 34].

To realize this rich variety of states, one obviously needs to *understand* and *control* the interaction between the confined species. As we know from the seminal works

of Olshanii [35] and Petrov, Holzmann, and Shlyapnikov [36, 37], confinement radically modifies the effective interaction between atoms [38]; in quasi-two-dimensions, in particular, confinement leads to the emergence of a bound state of energy $\epsilon = -|E^B|$ irrespective of the sign of the interactions of unconfined particles, and a corresponding broad scattering resonance at collision energies $\epsilon \sim |E^B|$ also appears. Consequently, due to the presence of this bound state, the effective interaction of low-energy quasiparticles is always repulsive [36, 39]. The aforementioned bound states originate from the peculiar scattering properties of two-dimensional systems [36, 40], and were indeed observed both in quasi-one and in quasi-two dimensions [8, 41–45].

In this work, we focus our attention on layered two-dimensional systems, sketched in Fig. 1, and explore how confinement influences interactions in such structures. To be specific, we consider atoms of two hyperfine states, $\alpha = \uparrow, \downarrow$, confined optically into quasi-two-dimensional layers within the xy plane. Having different magnetic moments, the separation $d_{\uparrow\downarrow}$ of the two hyperfine components can be controlled by a magnetic field gradient applied in the z direction. An alternative, and maybe even simpler way to separate the layers is by using spin-dependent optical lattices [46–48], through the application of vectorial light shifts.

For simplicity, we assume a simple parabolic confinement for each species,

$$\mathcal{H}_\alpha = \frac{\mathbf{p}^2}{2m} + \frac{m\,\omega_z^2}{2}\, z_\alpha^2 \,, \qquad (1)$$

with the z coordinates $z_\alpha \equiv z - z_\alpha^0$ measured from the centers of the layers, z_α^0, and with the natural length scale in the transverse direction set by the oscillator length $l_z \equiv \sqrt{\hbar/(m\omega_z)}$. We consider a short-ranged s-wave interaction between each hyperfine components [49], $V_{\alpha\beta}(\mathbf{r} - \mathbf{r}')$, characterized by the three-dimensional scattering lengths $a_{\uparrow\uparrow}$, $a_{\uparrow\downarrow}$, and $a_{\downarrow\downarrow}$. As a first step, we determine the two-particle scattering wave functions and scattering amplitudes analytically. We find that, as a result of confinement, in the $\uparrow\downarrow$ channel bound interlayer molecular states of energy $E_{\uparrow\downarrow}^B$ emerge both for positive, $a_{\downarrow\uparrow} > 0$, and for negative scattering length, $a_{\downarrow\uparrow} < 0$ (see Fig. 2). As schematically shown in Fig. 1 (and later displayed in Fig. 4), these 'giant' molecular states extend over both layers simultaneously, somewhat similarly to electronic excitons in bilayer quantum well structures [16, 17]. Similar to the case of a single component [37], their presence implies a *repulsive* effective interaction between species $\uparrow$ and $\downarrow$ at low energies, $\epsilon \ll |E_{\uparrow\downarrow}^B|$, irrespective of the sign of $a_{\uparrow\downarrow}$.

As another consequence of confinement, an unexpected scattering resonance (quasi-bound state) appears at positive collision energies $\epsilon \sim |E_{\uparrow\downarrow}^B|$ (dashed line in Fig. 2) [50]. Furthermore, we find similar resonances near the edges of the transverse harmonic oscillator channels, $\nu \hbar \omega_z$, with channel index ν. Similar quasi-bound molecular states also exist for a single layer of atoms. There,

however these confinement-induced molecular states are extremely (logarithmically) broad in energy [37], and have therefore never been observed experimentally. In the layered arrangement studied here, however, the line widths of these molecular resonances are very sensitive to the layer separation, and become sufficiently sharp to be observable for appropriate separations. As we demonstrate through detailed many-body calculations for thermal bosons, the bound state and a quasi-bound state appear as separate, well-resolved lines in the shaking spectrum, induced by varying the separation $d_{\uparrow\downarrow}$ periodically in time.

The molecular resonances discussed here offer a route to control the interaction between different hyperfine components geometrically: Not only the line width, but also the energy of the interlayer molecular resonance depends sensitively on layer separation. Eventually, the energy of the molecular resonance approaches zero upon changing $d_{\uparrow\downarrow}$ and – for positive scattering length and tight confinement ($a_{\uparrow\downarrow}/l_z \sim 1$) a sharp *interlayer Feshbach resonance* emerges as a function of layer separation in the scattering amplitude of low energy particles, $\epsilon \ll \hbar \omega_z$. Thus, rather counterintuitively, one can induce an extremely *strong interaction* in the $\uparrow\downarrow$ channel by separating the two hyperfine species in space. Together with confinement-tuning, – used previously to control intraspecies interactions and to realize the Tonks–Girardeau gas [6, 51–53], – 'separation-tuning' would enable one to gain full, purely geometrical control of interacting, two-dimensional multicomponent systems, and opens a route to realizing novel interaction-driven quantum phases.

Separation tuning has also been predicted to lead to interaction resonances in quasi-one-dimensional gases, exhibiting double scattering resonances as a function of the layer separation, in case of positive scattering lengths [54]. However, the bilayer geometry discussed here exhibits rather distinct features, due to the peculiarities of the two-dimensional scattering, such as the logarithmic energy broadening of scattering resonances, and the a finite lifetime of the associated molecular states, depending sensitively the layer separation. Our work also goes beyond the few-body calculation of Ref. 54 in that it discusses many-body aspects of these molecular states by determining the associated peaks in a modulation spectroscopy experiment.

II. TWO-PARTICLE SCATTERING

We start our analysis by studying the scattering of two particles on each other and determining the two-particle scattering states. Many-body effects shall be discussed in Sec. IV in case of a dilute Bose gas [55].

The scattering process of particles in layers α and β is governed by the Hamiltonian $\mathcal{H}_{\alpha\beta} = \mathcal{H}_\alpha + \mathcal{H}_\beta + V_{\alpha\beta}$, and can be greatly simplified by transforming into relative
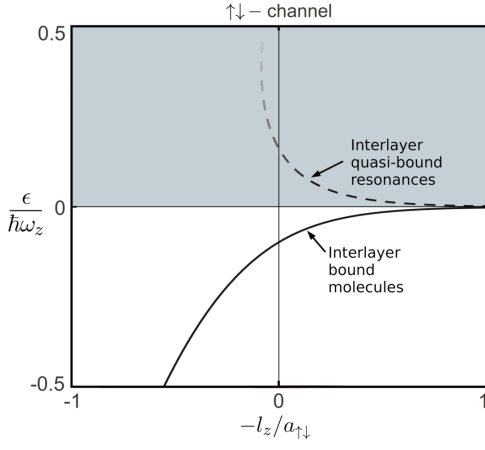
FIG. 2. (Color online.) Energy of the interlayer molecule in units of confinement energy, $\hbar\omega_z$, as a function of the oscillator length of the confining potential, l_z, divided by the three-dimensional scattering length, $a_{\uparrow\downarrow}$. The dashed line indicates the position of the corresponding resonance.

and center of mass (COM) coordinates. Defining

$$z \equiv z_\alpha - z_\beta, \qquad Z \equiv \frac{z_\alpha + z_\beta}{2}, \tag{2}$$

and likewise introducing in plane relative ($\vec{\rho}$) and center of mass coordinates ($\mathbf{R}$), the center of mass and relative motions decouple completely for the parabolic confinement considered, and the Hamiltonian can be divided into relative (rel) and center of mass (COM) parts as

$$\mathcal{H}_{\mathrm{rel}} = \frac{\mathbf{p}_\rho^2 + p_z^2}{m} + \frac{m\omega_z^2}{4}z^2 + V_{\alpha\beta}(\vec{\rho}, z - d_{\alpha\beta}),$$
$$\mathcal{H}_{\mathrm{COM}} = \frac{\mathbf{p}_\mathbf{R}^2 + p_Z^2}{4m} + m\omega_z^2 Z^2,$$

where $d_{\alpha\beta}$ denotes the separation between the layers of atoms β and α [56]. All non-trivial physics is now contained in the relative motion of the particles, governed by $\mathcal{H}_{\mathrm{rel}}$, which describes the motion of a particle of reduced mass $m/2$, confined into quasi-two dimensions by a parabolic potential, and scattered by the interaction potential, as shown in Fig. 3(a). Notice that for the $\uparrow\uparrow$ and $\downarrow\downarrow$ channels the delta potential induced by the atom-atom interaction is at the minimum of the parabolic confinement, while in the $\uparrow\downarrow$ channel it is shifted to $z = d_{\uparrow\downarrow}$.

In the absence of interactions, the two particles' wave function in the z direction can be expressed as $\Psi \sim \varphi_N(\sqrt{2}Z)\varphi_\nu(z/\sqrt{2})$, with φ_ν denoting the usual harmonic oscillator wave functions, and N and ν the center of mass and relative motions' quantum numbers, respectively. Even in the presence of interactions, the center of mass motion remains trivial, and the two-particle eigenstates can still be decomposed as

$$\tilde{\Psi} \sim \varphi_N(\sqrt{2}Z)\, e^{i\mathbf{Q}\mathbf{R}} \cdot \Psi_{\mathrm{rel}}(\vec{\rho}, z),$$

where $\mathbf{Q}$ denotes the total momentum of the particles and Ψ_{rel} stands for the non-trivial relative part of the
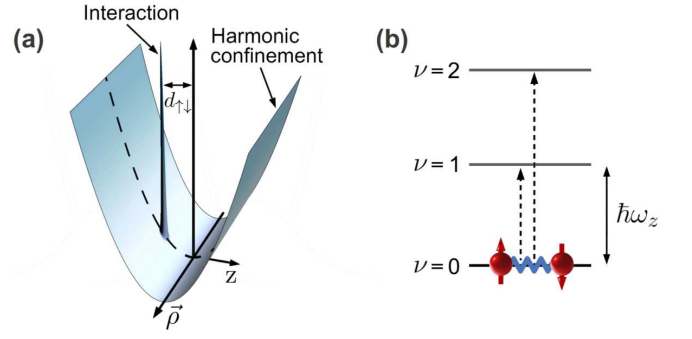

FIG. 3. (Color online.) (a) Interaction and harmonic trapping potential in relative coordinates of two particles of opposite spins. (b) The interaction potential mixes the relative harmonic oscillator quantum channels, ν, by introducing real and virtual transitions between them. These virtual transitions induce scattering resonances at energies close to the harmonic oscillator thresholds, $\hbar\nu\omega_z$.

wave function, governed by $\mathcal{H}_{\mathrm{rel}}$ [57]. The total energy of the two particles can therefore be expressed as a sum of the energy of the relative motion, ϵ, and that of the COM motion,

$$E = \epsilon + E_{\mathrm{COM}},$$

with $E_{\mathrm{COM}} = \mathbf{Q}^2/4m + N\hbar\omega_z$.

A. Scattering states

In the rest of this section, we shall focus only on the non-trivial relative motion, and consider the scattering of two incoming particles with opposite momenta $\pm\mathbf{q}$ in the relative harmonic oscillator channel ν. This pair of particles can scatter into channel ν' provided that the outgoing channel is 'open', i.e. $\nu'\hbar\omega_z$ is less than the energy of the relative motion, $\epsilon = \hbar^2\mathbf{q}^2/m + \nu\hbar\omega_z$.

The corresponding two-dimensional scattering processes are characterized by the dimensionless scattering amplitudes, $f_{\alpha\beta}^{\nu\nu'}$, governing the long distance ($\rho \gg l_z$) behavior of the scattering eigenstates $\Psi_{\alpha\beta}^{\nu,\epsilon}$ of the relative Hamiltonian [37],

$$\Psi_{\alpha\beta}^{\nu,\epsilon}(\mathbf{r}) \approx \phi_\nu(z)e^{i\mathbf{q}\vec{\rho}} - \sum_{\nu'} f_{\alpha\beta}^{\nu\nu'}(\epsilon)\sqrt{\frac{i}{8\pi q_{\nu'}\rho}} e^{iq_{\nu'}\rho}\phi_{\nu'}(z), \tag{3}$$

where $q_{\nu'} = \sqrt{m(\epsilon - \nu'\hbar\omega_z + i0^+)}/\hbar$ denotes the momenta in the outgoing channels and ϕ_ν stands for the properly normalized relative wave function, $\phi_\nu(z) = \varphi_\nu(z/\sqrt{2})/2^{1/4}$ [58]. The scattering amplitude $f_{\alpha\beta}^{\nu\nu'}$ is related to the scattering cross-section of $\nu \to \nu'$ transitions [59]

$$\sigma_{\alpha\neq\beta}^{\nu\to\nu'}(q) = \frac{|f_{\alpha\beta}^{\nu\nu'}(\hbar^2q^2/m)|^2}{4\,q} \tag{4}$$

and, being dimensionless, it only depends on the three dimensionless variables $\epsilon/\hbar\omega_z$, $d_{\alpha\beta}/l_z$ and $a_{\alpha\beta}/l_z$.

To determine the amplitudes $f_{\alpha\beta}^{\nu\nu'}$, we construct the two-particle scattering states. We first notice that being a scattering state, $\Psi_{\alpha\beta}^{\nu,\epsilon}$ satisfy the Lippmann–Schwinger equation [60],

$$\Psi_{\alpha\beta}^{\nu,\epsilon}(\mathbf{r}) = \phi_\nu(z)e^{i\mathbf{q}\vec{\rho}} - \frac{m}{\hbar^2}\int d^3r'\, G_\epsilon^{(0)}(\mathbf{r},\mathbf{r}')V_{\alpha\beta}(\mathbf{r}')\Psi_{\alpha\beta}^{\nu,\epsilon}(\mathbf{r}'). \quad (5)$$

Here $\mathbf{r} = (\vec{\rho}, z)$, and $G_\epsilon^{(0)}$ denotes the retarded Green's function of the non-interacting confined system, satisfying $(\epsilon - \mathcal{H}_{\mathrm{rel}}^0)\, G_\epsilon^{(0)}(\mathbf{r},\mathbf{r}') = \delta(\mathbf{r}-\mathbf{r}')$, and expressed in terms of modified Bessel functions as

$$G_\epsilon^{(0)}(\mathbf{r},\mathbf{r}') = \frac{1}{2\pi}\sum_{\nu=0}^{\infty}\phi_\nu(z)\phi_\nu(z')K_0(-iq_\nu|\vec{\rho}-\vec{\rho}'|). \quad (6)$$

The second term of Eq. (5) describes the scattered part of the wave function, $\delta\Psi_{\alpha\beta}^{\nu,\epsilon}$. For the short-ranged potential considered here Eq. (5) immediately yields

$$\delta\Psi_{\alpha\beta}^{\nu,\epsilon} = A\, G_\epsilon^{(0)}(\mathbf{r}, d_{\alpha\beta}\,\hat{\mathbf{z}}). \quad (7)$$

The value of the unknown proportionality constant (i.e., the amplitude of the scattered wave) can be determined by inspecting the wave function around the point of interaction at short distances, $\delta r \equiv |\mathbf{r} - d_{\alpha\beta}\,\hat{\mathbf{z}}| \ll l_z$. At such short distances the propagation of the particles is essentially free, and correspondingly, $G_\epsilon^{(0)}$ exhibits the well-known $1/\delta r$ singularity of the three-dimensional free propagator,

$$G_\epsilon^{(0)}(\mathbf{r}, d_{\alpha\beta}\hat{\mathbf{z}}) \approx \frac{1}{4\pi}\left(\frac{1}{\delta r} + \frac{w_{\alpha\beta}(\epsilon/\hbar\omega_z)}{\sqrt{2\pi}l_z} + \ldots\right). \quad (8)$$

Here $w_{\alpha\beta}(\epsilon/\hbar\omega_z)$ are energy (and separation) dependent constants [37], incorporating the effects of confinement. They can be expressed from Eq. (6) by carefully separating the $1/\delta r$ singularity (see Appendix A) [37, 38], yielding

$$w_{\alpha\beta}(x) = \lim_{\bar{\nu}\to\infty}\left[c_{\bar{\nu}} - \sum_{\nu=0}^{2\bar{\nu}-1}\frac{\phi_\nu^2(d_{\alpha\beta})}{\phi_0^2(0)}\log\left(\frac{\nu-x-i0^+}{2}\right)\right], \quad (9)$$

with $c_\nu \equiv 2\sqrt{\frac{\nu}{\pi}}\log\frac{\nu}{e^2}$.

The amplitude of the scattered part of the wave function in Eq. (7) can now be determined from the observation [37] that at short distances, $\delta r \ll l_z$, confinement does not modify the interactions, and therefore, beyond the range of the inter-particle interaction – only a few Bohr radius in practice – the relative wave function of the two particles must have the same asymptotics as in three dimensions,

$$\Psi_{\alpha\beta}(\mathbf{r}) \sim 1 - \frac{a_{\alpha\beta}}{\delta r} + \mathcal{O}(\delta r)\,. \quad (10)$$

Comparing this expansion to the asymptotic form (8) and to Eq. (7), we can determine the unknown amplitude in Eq. (7), and obtain the exact solution of the two-particle scattering problem [61],

$$\Psi_{\alpha\beta}^{\nu,\epsilon}(\mathbf{r}) = e^{i\mathbf{q}\vec{\rho}}\phi_\nu(z) - \frac{4\pi\, a_{\alpha\beta}\,\phi_\nu(d_{\alpha\beta})}{1 + \frac{a_{\alpha\beta}}{\sqrt{2\pi}\,l_z}\,w_{\alpha\beta}(\epsilon/\hbar\omega_z)}\, G_\epsilon^{(0)}(\mathbf{r}, d_{\alpha\beta}). \quad (11)$$

B. Scattering amplitudes, bound molecular states

The scattering wave function, Eq. (11), contains a lot of information. First, it allows us to determine the *scattering amplitudes* by comparing the asymptotic form of $G_\epsilon^{(0)}(\mathbf{r})$ in (11) to the usual expansion of the scattering states, Eq. (3). This yields the quasi-two-dimensional scattering amplitudes

$$f_{\alpha\beta}^{\nu\nu'}(\epsilon) = \frac{4\pi a_{\alpha\beta}\,\phi_\nu(d_{\alpha\beta})\phi_{\nu'}(d_{\alpha\beta})}{1 + \frac{a_{\alpha\beta}}{\sqrt{2\pi}\,l_z}\,w_{\alpha\beta}(\epsilon/\hbar\omega_z)} \quad (12)$$

in the open channels. The numerator of this expression conforms to the expectation that, to leading order, the scattering amplitude should be proportional to the first order matrix element of the (renormalized) interaction with the harmonic oscillator eigenstates of the channels involved.

This naive result is, however, modified by virtual transitions between transverse channels, described by the functions $w_{\alpha\beta}$ in the denominator of (12). These functions, given by Eq. (9), determine the positions of bound states and resonances in the presence of confinement: these latter emerge, whenever the real part of the denominator in Eq. (12) becomes zero. While for scattering within the same spin channels we have $d_{\uparrow\uparrow} = d_{\downarrow\downarrow} = 0$, and Eq. (12) reduces to the expression of Ref. 37, for the spin $\uparrow\downarrow$ channel $f_{\uparrow\downarrow}(\epsilon)$ depends sensitively on the distance $d_{\uparrow\downarrow}$ between the two layers through the relative wave functions, ϕ_ν, appearing in Eq. (9).

As a peculiar feature of quasi-two-dimensional scattering, the scattering amplitudes always have a pole at some $\epsilon \equiv E_{\alpha\beta}^B < 0$ corresponding to a *bound molecular state*, for *any* value and sign of the three-dimensional scattering length. Mathematically, this follows from the logarithmic singularity of $w_{\alpha\beta}$ at small energies, $w_{\alpha\beta} \sim \phi_0^2(d_{\alpha\beta})\left(-\ln|\epsilon/(\hbar\omega_z)| + i\Theta(\epsilon)\right)$, related to two-dimensional propagation. The presence of this logarithmic singularity necessarily implies the emergence of a bound state (pole in $f_{\alpha\beta}^{00}$). Specifically, for small negative scattering lengths the molecular bound state is located approximately at

$$E_{\alpha\beta}^B \propto -\hbar\,\omega_z\, e^{-1/\left(|a_{\alpha\beta}|\phi_0^2(d_{\alpha\beta})\right)}. \quad (13)$$

Its wave function can easily be obtained from Eq. (5), leading to the simple form

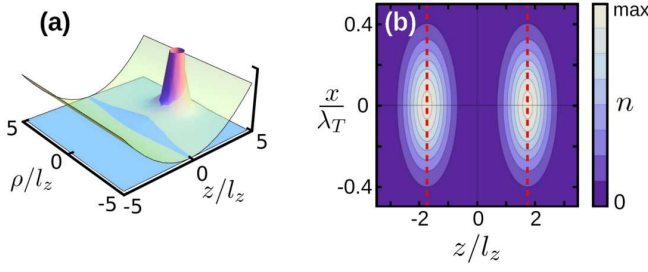$$\Psi_{\alpha\beta}^B(\mathbf{r}) = G_{E_{\alpha\beta}^B}^{(0)}(\mathbf{r}, d_{\alpha\beta})\,.$$

FIG. 4. (Color online.) Visualization of an intralayer molecular state, at a separation $d_{\uparrow\downarrow}/l_z = 3.5$. (a) Bound state wave function $\Psi^B_{\uparrow\downarrow}$, in relative coordinates of the atoms, displaying the well-known $1/(4\pi\,\delta r)$ singularity of unconfined bound states at the point of interaction. The harmonic confining potential is also shown. (b) Real space density $n(\mathbf{r}) = \int d^3\mathbf{r}'\,\|\tilde{\Psi}_{\alpha\beta}(\mathbf{r},\mathbf{r}')\|^2$ of the two-particle bound state $\tilde{\Psi}_{\alpha\beta}(\mathbf{r},\mathbf{r}')$ in the (x,z) plane of the laboratory frame. Only a tiny part of the wave function tunnels into the intermediate region. For the COM part of the wave function we assumed a temperature $k_B T = 0.1\,\hbar\omega_z$ and a Gaussian in plane wave function localized within the thermal de Broglie wavelength.

The interlayer molecular states are visualized in Fig. 4, showing the bound state wave function in relative coordinates, as well as their density in the laboratory frame. They clearly display a double-peak feature at non-zero separation, consistent with naive expectations. We emphasize again that the appearance of these bound states for negative three-dimensional scattering lengths is the special feature of two-dimensional scattering [37].

C. Quasi-bound molecular states

For energies $\epsilon > 0$ no bound state can exist since any molecule can decay into the two-particle continuum, leading to a finite imaginary part of the scattering amplitudes. Nevertheless, the scattering of atoms still becomes structured due to confinement, and exhibits resonances [37]. The low energy scattering amplitude, e.g., can be expressed in terms of the bound state's energy as

$$f^{00}_{\alpha\beta}(\epsilon \approx 0) \approx \frac{4\pi}{\log\big|E^B_{\alpha\beta}/\epsilon\big| + i\,\pi\,\Theta(\epsilon)}, \qquad (14)$$

and exhibits a very broad resonance at an energy $\epsilon = |E^B_{\alpha\beta}|$ [37]. Similarly, $f_{\alpha\beta}(\epsilon)$ displays resonances of finite width each time the real part of the denominator of Eq. (12) crosses zero, signifying *quasi-bound states* of finite lifetime. These resonances correspond the *unstable* molecular states, which then decay into the continuum.

The energies of these quasi-bound molecular states are displayed in Fig. 5 for some typical confinement parameters as a function of $l_z/a_{\alpha\beta}$. Surprisingly, the interlayer scattering (solid line) displays features completely absent in intralayer scattering (dashed lines). While for intralayer scattering $\nu = 0 \rightarrow \nu = 1$ relative quantum number transitions are forbidden by reflection symmetry

(as well as by Bose statistics in case of colliding bosons), such interlayer processes are allowed once $d_{\uparrow\downarrow} \neq 0$, and they amount in the emergence of a novel quasi-bound molecular state (resonance) at an energy

$$(E^1_{\uparrow\downarrow} - \hbar\omega_z) \;\propto\; -\hbar\omega_z\, e^{-1/\left(|a_{\uparrow\downarrow}|\phi^2_1(d_{\uparrow\downarrow})\right)}. \qquad (15)$$

Importantly, while the weight and the binding energy of this molecular resonance is determined by $\phi^2_1(d_{\uparrow\downarrow})$, its decay rate is proportional to $\phi^2_0(d_{\uparrow\downarrow})$,

$$f^{00}_{\uparrow\downarrow}(\epsilon \lesssim \hbar\omega_z) \approx \frac{4\pi}{\frac{\phi^2_1(d_{\alpha\beta})}{\phi^2_0(d_{\alpha\beta})}\cdot\log\big|E^1_{\uparrow\downarrow}/\epsilon\big| + i\,\pi}. \qquad (16)$$

Therefore, increasing the separation between the two layers of atoms, one can make the quasi-bound state sharper and sharper — at the cost of somewhat decreasing its weight (see also the inset of Fig. 5). Similar interlayer quasi-bound states of energy $E^\nu_{\uparrow\downarrow}$ appear close to every threshold, $\epsilon \approx \nu\,\hbar\omega_z$, and can turn to a narrow resonance as one increases further the layer separation $d_{\uparrow\downarrow}$.

We should emphasize that Fig. 5 displays only the relative energy ϵ of the molecular states in the center of mass frame. The total energy of two particles is, however, given as a sum of the energy associated with their relative and center of mass motions, $E = \epsilon + E_{\mathrm{COM}}$. Accordingly, the bound state spectrum in Fig. 5 is replicated at energies $E \rightarrow \epsilon + N\hbar\omega_z$, corresponding to excited molecular bound states with an oscillating center of mass motion along the z direction. One can thus observe molecular bound states even at positive total energies E in the $N > 0$ channels, as long as the COM and relative motions are completely decoupled [62].

III. GEOMETRIC INTERACTION CONTROL

In this section, we discuss in the case of a degenerate Bose gas, how the emergent interlayer resonances can be exploited to tune interspecies interactions *independently*, simply by changing the layer separation. In a strongly confined ($k_B T \ll \hbar\omega_z$) gas, the effective interaction is approximately proportional to the scattering amplitude at the corresponding energy $\epsilon = 2\mu$,

$$g_{\uparrow\downarrow} \simeq \frac{\hbar^2}{m}\, f^{00}_{\uparrow\downarrow}(2\mu),$$

with the chemical potential μ [37, 38]. Fig. 6(a) shows the scattering amplitude in the $\uparrow\downarrow$-channel as a function of layer separation for fixed energies, $0 < \epsilon \ll \omega_z$. As one would naively expect, for the parameters chosen, the interaction initially decreases with increasing separation, due to the ever weaker overlap between the atomic clouds of the layers. Then, a sharp Feshbach-resonance-like structure emerges as a quasi-bound state approaches the energy of the incoming particles, leading to a very strong interaction between the two species.

We find similar Feshbach-like resonances at fixed layer separations, shown in Fig. 7, as the three-dimensional scattering amplitude $a_{\uparrow\downarrow}$ is varied through the confinement-induced resonance. Crossing the resonance, the effective interaction turns from repulsive to attractive, reaching its universal, purely imaginary value of $f_{\uparrow\downarrow}^{00} = -4i$ on resonance.

Notice, that in contrast to single layer systems [37], these resonances appear *both* on the attractive and on the repulsive side of the three-dimensional Feshbach resonance, and, in a somewhat unusual way, they become the sharpest on the repulsive side, $a_{\uparrow\downarrow} > 0$. In addition, increasing layer separation leads to the emergence of quasi-bound molecular states at smaller and smaller values of the scattering lengths, $a_{\uparrow\downarrow} > 0$, as indicated in Figs. 5(b)-(e). The appearance of these states leads to confinement-induced resonances also at relatively small values of the scattering lengths, $a_{\uparrow\downarrow} \lesssim l_z$. Thus, geometrical interaction control shall be useful for reaching the strongly correlated regime in systems, where no magnetic Feshbach resonances are available and only moderate values of the scattering length can be reached [63].

IV. MODULATION EXPERIMENT

Despite the intense investigation of the negative energy bound states in recent spectroscopy experiments with single layer systems [43, 44], quasi-bound molecules remained elusive due to their very short lifetimes. In
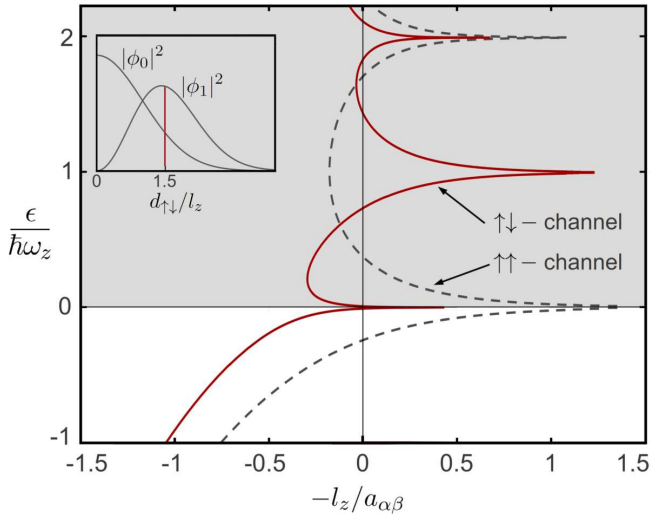

FIG. 5. (Color online.) Energies of bound and quasi-bound molecules in the $\uparrow\uparrow$ and $\downarrow\downarrow$ (dashed line), and in the $\uparrow\downarrow$-channel with layer separation $d_{\uparrow\downarrow}/l_z = 1.5$ (full line), in the vicinity of a three-dimensional Feshbach resonance of the scattering length $a_{\alpha\beta}$. Only the energy associated with the relative motion are shown. Inset: amplitudes $\phi_0^2(d_{\uparrow\downarrow})$ and $\phi_1^2(d_{\uparrow\downarrow})$ as functions of $d_{\uparrow\downarrow}/l_z$. The factor $\phi_1^2(d_{\uparrow\downarrow})$ determines the binding energy of the first quasi-bound molecule, while $\phi_0^2(d_{\uparrow\downarrow})$ is proportional to its lifetime.
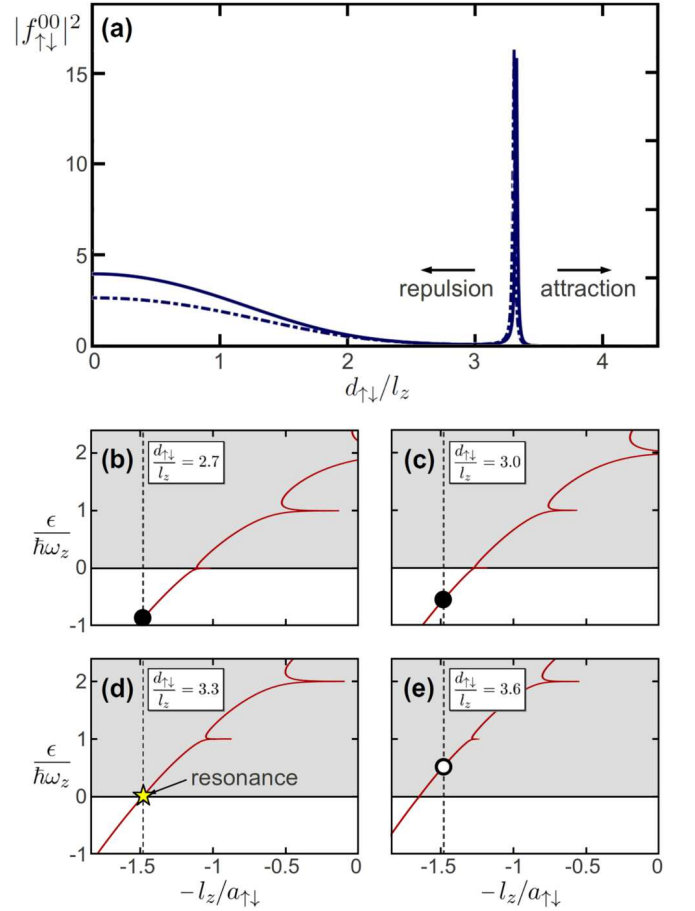

FIG. 6. (Color online.) (a) Scattering amplitude $f_{\uparrow\downarrow}^{00}$ as a function of the layer separation, $d_{\uparrow\downarrow}$, at a fixed scattering length $a_{\uparrow\downarrow} = 0.68\,l_z$ (indicated by dashed lines in (b)-(e)). The continuous and dashed curves correspond to energies $\epsilon/\hbar\omega_z = 0.05$ and 0.01, respectively. A sharp Feshbach resonance structure emerges at $d_{\uparrow\downarrow}/l_z = 3.3$, when the energy of incoming particles become resonant with a long-lived quasi-bound molecular state. (b)-(e) The energy of the bound and quasi-bound states (full and open circles, respectively) at increasing layer separations $d_{\uparrow\downarrow}/l_z = 2.7$, 3.0, 3.3 and 3.6. The interaction resonance in (a) corresponds to the appearance of a quasi-bound molecular state at zero energy, shown in (d). The energy of this state gets shifted to positive energies at larger separations, as depicted in (e).

bilayer gases considered here, however, interlayer quasi-bound molecules can be made exponentially long-lived simply by increasing the layer separation, and they can therefore be detected in simple shaking experiments. To demonstrate this, we determine the modulation spectrum of a strongly confined dilute Bose gas (with a temperature $k_B T \ll \hbar\omega_z$), excited by the simultaneous shaking of both layers in opposite directions. Such a shaking field can be conveniently produced either by applying a time dependent magnetic field gradient, or through periodically modulated vector light shifts in a spin-dependent optical potential [46]. coupled to a time dependent magnetic field gradient that shakes the layers in opposite di-
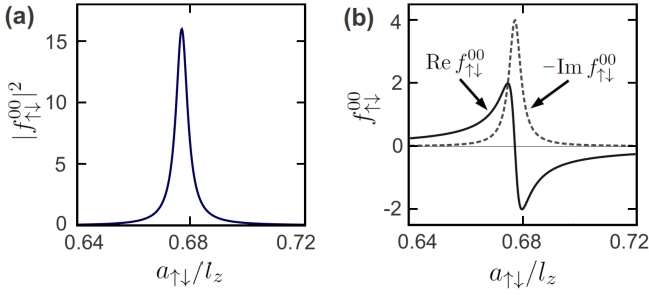
FIG. 7. (Color online.) Scattering amplitude $f_{\uparrow\downarrow}^{00}$ in terms of the scattering length $a_{\uparrow\downarrow}$ in the vicinity of the resonance shown in Fig. 6(a), but with the layer separation fixed at $d_{\uparrow\downarrow} = 3.3 l_z$. (a) The scattering amplitude exhibits a strong peak as $a_{\uparrow\downarrow}$ is tuned through the Feshbach-like resonance at $a_{\uparrow\downarrow} \approx 0.68 \, l_z$. (b) Crossing the resonance, interactions turn from repulsive to attractive, exhibiting a large imaginary part, due to the finite lifetime of the resonant quasi-bound molecule.

rections. To account for many-body effects, we describe the gas in terms of the second quantized Hamiltonian,

$$H = \int \mathrm{d}^3\mathbf{r}\{\sum_\alpha \psi_\alpha^\dagger(\mathbf{r})(\mathcal{H}_\alpha - \mu_\alpha)\psi_\alpha(\mathbf{r}) \qquad (17)$$
$$+ \sum_{\alpha,\beta} \frac{g_{\alpha\beta}}{2}\, \psi_\alpha^\dagger(\mathbf{r})\psi_\beta^\dagger(\mathbf{r})\psi_\beta(\mathbf{r})\psi_\alpha(\mathbf{r})\},$$

with the fields ψ_α annihilating particles in layer α, and the chemical potentials $\mu_\alpha < 0$ setting the densities. The interaction parameters $g_{\alpha\beta}$ are related to the three-dimensional scattering lengths through appropriate renormalization [38]. Shaking is described by the modulation of the Hamiltonian $\mathcal{H}_\alpha$,

$$\delta\mathcal{H}_\alpha(t) = -h_\alpha \cos(\omega t)\, z_\alpha/l_z, \qquad (18)$$

with modulation frequency ω, and the fields h_α characterizing the amplitudes of shaking for the two hyperfine components. Due to the selection rules imposed by harmonic confinement, shaking induces $n \leftrightarrow (n+1)$ intralayer transitions within each layer, to leading order. In a strongly confined Bose gas, dominantly $n = 0 \to 1$ transitions will be excited, since the $n > 0$ levels are essentially unpopulated. Decomposed in terms of center of mass (N) and relative (ν) quantum numbers, these correspond to pair excitations $(N, \nu) = (0,0) \to (1,0)$ and $(0,0) \to (0,1)$ [64]. Therefore, shaking not only allows to excite thermal particles to higher intrawell bands (at energy $\hbar\omega_z$), but – through the interaction with other thermal bosons – it can also excite bound and quasi-bound molecular states.

In particular, $(N, \nu) = (0,0) \to (0,1)$ transitions excite the $\uparrow\downarrow$ interlayer quasi-bound molecule of energy $E_{\uparrow\downarrow}^1$, close to the $\hbar\omega_z$ threshold (open circle in Fig. 9(b)). The other, $(N, \nu) = (0,0) \to (1,0)$ excitation creates transitions to molecular bound states in the $\uparrow\uparrow$ and $\downarrow\downarrow$-channels. Due to the center of mass energy $N\hbar\omega_z$, the

energy of these bound states can get shifted to positive values, $E_{\uparrow\uparrow}^B \to E_{\uparrow\uparrow}^B + \hbar\omega_z$ (and $E_{\downarrow\downarrow}^B + \hbar\omega_z$). We therefore expect peaks at all these energies in the absorption spectrum [65].

To verify these expectations, we calculated the imaginary part of the shaking susceptibility, $\chi_\alpha''(\omega)$, using field theoretical methods. Neglecting vertex corrections, $\chi_\alpha(\omega)$ is given by the 'dressed' bubble diagrams in Fig. 8(a). This quantity is directly related to the rate of energy absorption in layer α, given by $\dot{\epsilon}_\alpha(\omega) = h_\alpha^2 \omega \chi_\alpha''(\omega)/2$. During their propagation, particles excited by lattice modulations go through virtual transitions to bound and quasi-bound states with other particles in the thermal gas. Interactions between the excited particles and the thermal gas are incorporated in the dressed propagators (heavy lines), through self-energy contributions. To compute this, we expand the fields ψ_α in terms of harmonic oscillator wave functions. $\psi_\alpha(\mathbf{r}) \propto \sum_n \int d^2q\, \varphi_n(z - z_\alpha^0)\, e^{i\mathbf{q}\vec{\rho}} a_{\alpha n}(\mathbf{q})$. In this basis, the dressed retarded propagator of particles in layer α is given by

$$(G_R^{-1})_\alpha^{nn'}(\omega, \mathbf{q}) = \omega + i0^+ + \frac{\hbar q^2}{2m} + n\omega_z\, \delta_{nn'} + \frac{1}{\hbar}\Sigma_\alpha^{nn'}(\omega, \mathbf{q}),$$

with the self-energy $\Sigma_\alpha^{nn'}$ accounting for interactions with thermal particles (see Fig. 8(b)), creating transitions between harmonic oscillator levels $n \to n'$.

We compute the self-energies within the T-matrix approximation by summing up the complete ladder diagrams for the T-matrix (vertex function), and solving the corresponding Bethe-Salpeter equations (see Fig. 8(c)). In the absence of thermal particles, the T-matrix approximation becomes exact, and gives an expression identical to the scattering amplitudes in Eq. (12), up to a nor-
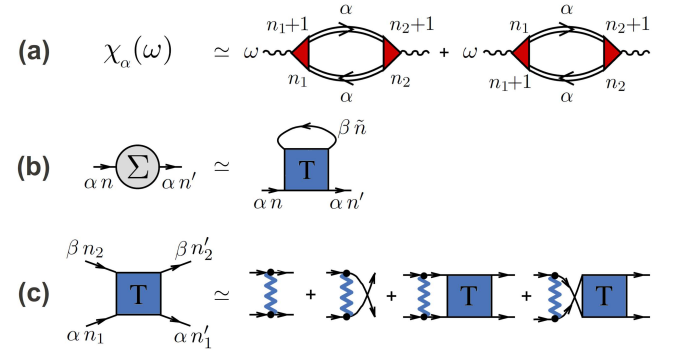

FIG. 8. (Color online.) Feynman diagrams determining the shaking spectrum: (a) Shaking susceptibility, as calculated within linear response theory and neglecting vertex corrections. Double lines indicate propagators dressed by self-energy corrections (b), whereas red triangles stand for shaking vertices. (b) Self-energy corrections within the T-matrix approximation. (c) Bethe-Salpeter equations of the many-body T-matrix, approximated as a sum up ladder diagrams. Full lines indicate bare propagators, dashed lines refer to the bare coupling.
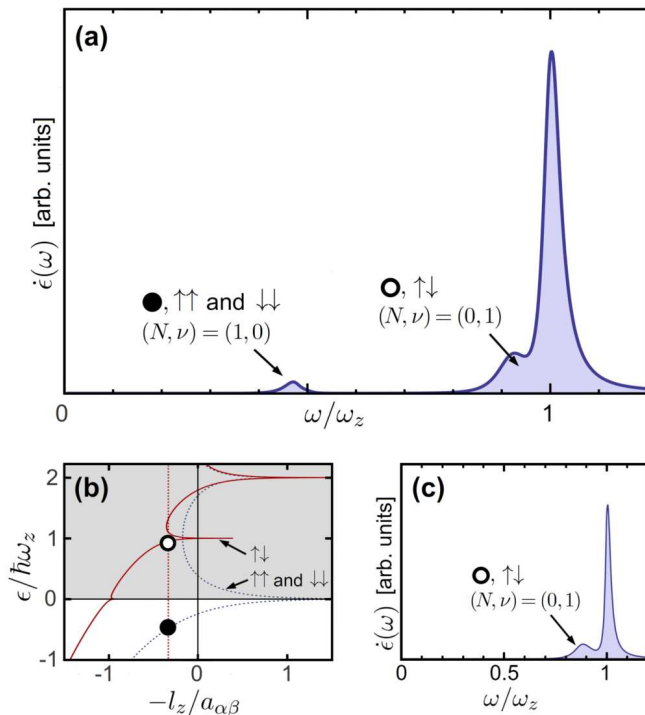
FIG. 9. (Color online.) (a) Shaking absorption spectrum at equal interaction strengths $a_{\alpha\beta}/l_z = 3$, and layer separation $d_{\uparrow\downarrow}/l_z = 2.5$. Center of mass ($N$) and relative ($\nu$) quantum numbers of the peaks related to bound and quasi-bound molecular states are indicated by full and open circles, respectively, also shown in (b). [Physical parameters: $|\mu_\uparrow| = |\mu_\downarrow| = k_B T/3$, $k_B T = 0.03\,\hbar\omega_z$.] (c) In the absence of interlayer interactions ($a_{\uparrow\uparrow} = a_{\downarrow\downarrow} = 0$), the bound states in the $\uparrow\uparrow$ and $\downarrow\downarrow$-channels disappear, and the corresponding peak vanishes from the modulation spectrum. [Parameters of the inset: $a_{\uparrow\downarrow} = 2.6\,l_z$, $|\mu_\uparrow| = |\mu_\downarrow| = k_B T/3$, $k_B T = 0.06\,\hbar\omega_z$.]

malizing constant. In a dilute Bose gas, however, the T-matrix contains additional many-body contributions, accounting for screening effects [38]. Details of these many-body calculations are given in Appendix B, here we just summarize the main results.

Fig. 9(a) displays the numerically computed shaking spectrum for some typical parameters in the cross-over regime, $a_{\alpha\beta} \sim l_z$ and $d_{\uparrow\downarrow} \sim l_z$. For simplicity, we assumed shaking fields $h_\uparrow = h_\downarrow$, and repulsive three-dimensional scattering lengths of equal size in all three scattering channels, $a_{\alpha\beta} = a$. Three peaks are clearly distinguishable in the spectrum. The largest peak at $\omega \approx \omega_z$ corresponds the direct subband transitions within the same layer, and has an amplitude directly proportional to the boson density. We also observe, however, two smaller peaks. These are due to two-body processes, therefore their intensities are proportional to the *square* of the boson densities. The peak next to the large quasiparticle excitation peak is due to the quasi-bound molecular state in the $\uparrow\downarrow$-channel at energy $E^1_{\uparrow\downarrow}$, indicated by the empty circle in Fig. 9(b). As expected, for separations $d \sim l_z$

this peak is indeed sharp enough and can be identified unambiguously within the shaking spectrum. Although this quasi-bound resonance may appear relatively weak at a first sight for the thermal gas studied here, it is expected to get more pronounced at higher densities, as the system is driven towards quantum degeneracy – a regime beyond the reach of the approximations used here.

The peak at even smaller frequencies has an entirely different origin, and is attributed to a transition into the $\uparrow\uparrow$ or $\downarrow\downarrow$ intralayer bound states combined with a center of mass excitation, $N = 0 \rightarrow 1$ (full circle in Fig. 9(b)). Notice that – to leading order – a direct transition to the bound state due to shaking is forbidden by symmetry (parity), and therefore excitation of a center of mass oscillation is necessary to observe the $E^0_{\uparrow\uparrow}$ and $E^0_{\downarrow\downarrow}$ bound states. This peak is expected to split up for $a_{\uparrow\uparrow} \neq a_{\downarrow\downarrow}$, and it vanishes if we set $a_{\uparrow\uparrow}, a_{\downarrow\downarrow} \rightarrow 0$ (see Fig. 9(c)). The bound state in the $\uparrow\downarrow$ scattering gives a tiny contribution for these parameters, and is practically not visible in Figs. 9(a, c).

Finally, we mention that time-modulation of the scattering lengths instead of the layer separation may provide an alternative experimental procedure of exciting the bound and quasi-bound molecular states, most probably leading to smaller quasi-particle contributions. Unlike the modulation of the layer separation, this perturbation couples the $(N, \nu) = (0, 0)$ state to a large number of harmonic oscillator channels, and it is therefore likely to excite a number of molecular states at higher energies as well.

V. CONCLUSIONS AND OUTLOOK ON EXPERIMENTS

In the preceding sections, we have studied theoretically how confinement modifies interactions in bilayer gases of ultracold atoms. We determined the two-particle scattering amplitudes and demonstrated the existence of confinement-induced interlayer molecular bound states for all values of the the scattering lengths $a_{\uparrow\downarrow}$. Rather counter-intuitively, these exciton-like interlayer molecular states exist even at layer separations several times larger than the oscillator length l_z of the confining potential, in a regime, where the overlap between the clouds is almost negligible.

At positive energies, $\epsilon > 0$, the scattering amplitudes exhibit confinement induced resonances of finite width, attributed to quasi-bound molecular states of finite lifetime. Here we have also demonstrated the existence of a novel kind of quasi-bound interspecies molecular states at energies $\epsilon \simeq \hbar\omega_z$, absent in single layer systems. These resonances are due to virtual processes, whereby two colliding atoms bind into a virtual interlayer molecular state, which then decays into the continuum. The energy and lifetime of these quasi-bound molecular states depend sensitively on the layer separation $d_{\uparrow\downarrow}$ and on the scattering lengths $a_{\uparrow\downarrow}$ (see Sec. III). The sensitivity

of these novel resonances can be exploited to *engineer* the interaction between the two species: rather counter-intuitively, the interaction between two species of atoms can be made resonant by spatially *separating* the two species. The geometrical interaction control proposed here is efficient also for moderate values of the scattering lengths $a_{\uparrow\downarrow}$, can therefore be used in a range of atomic species, and thus paves the way to realizing novel strongly-correlated many-body phases.

Ordinary confinement induced resonances in quasi-two-dimensional systems are extremely broad and, in fact, have never been detected before. The novel inter-species resonance, however, is getting sharper as the two species are separated and, as we have demonstrated for the case of a strongly confined dilute Bose gas in Sec. IV, it is observable in a simple shaking experiment, where it appears as a clearly distinguishable absorption peak. Due to its two-body character, the intensity of the corresponding absorption peak is proportional to the square of the boson density, and is expected to become more pronounced as the system is driven towards quantum degeneracy.

For an experimental observation of the above effects, one needs to reach the regime, where all natural length scales are of the same order, $a_{\alpha\beta} \sim l_z \sim d_{\uparrow\downarrow}$. One way to reach this regime is to decrease l_z, by applying extremely strong trapping frequencies, or by using heavy atoms (such as ^{87}Rb) [66]. No such a strong confinement is needed, however, for atoms with interspecies Feshbach resonances, where the scattering length $a_{\uparrow\downarrow}$ can be tuned by magnetic fields to large enough values at standard trapping frequencies, $\omega_z = 10-100$ kHz [67]. Although in case of bosonic species, broader resonances between hyperfine levels of the same atom are relatively rare [68, 69], they are much more common and widely used in the case of bosonic mixtures, such as ^{7}Li–^{87}Rb, ^{39}K–^{87}Rb and ^{41}K–^{87}Rb systems [69–73]. Although for species of unequal masses the center-of mass and relative motion decouple only for equal confinement frequencies, we do not expect our results to change dramatically even if these two confinement frequencies are different [74]. In these systems the regime $a_{\uparrow\downarrow} \sim l_z$ is thus readily accessible.

The ideas presented here are not limited to bosonic systems. Our results on two-particle scattering in the vacuum, discussed in Sec. II, apply to dilute Fermi gases as well. In the Fermionic case, s-wave scattering between identical fermion species is inactive due to the Pauli principle ($a_{\uparrow\uparrow}, a_{\downarrow\downarrow} \to 0$). Since fermionic systems (such as ^{6}Li and ^{40}K) have sufficiently broad and widely used Feshbach resonances, the regimes required to observe the effects of interlayer quasi-bound states can be easily reached within standard experiments. Fermionic gases are therefore promising candidates for detecting interlayer quasi-bound molecules in modulation experiments, and for implementing the geometrical interaction control discussed here. In the fermionic case, many-body effects can be accounted for by similar methods to those presented in Sec. IV [38], and could lead to several exotic

phenomena in a Fermi degenerate gases such as exciton condensation [16, 17].

Appendix A: Short distance asymptotics of the retarded Green's function

We determine the constant part of $G_\epsilon^{(0)}$ at short distances, by comparing Eqs. (6) and (8), leading to

$$w_{\alpha\beta} = \lim_{\rho \to 0} \left(2 \sum_{\nu=0}^\infty \frac{\phi_\nu^2(d_{\alpha\beta})}{\phi_0^2(0)} K_0\left(-iq_\nu\rho\right) - \frac{\sqrt{2\pi}l_z}{\rho} \right),$$

with $\phi_0^2(0) = 1/(\sqrt{2\pi}l_z)$. To simplify this expression, we choose a large integer, $\overline{\nu} \gg 1$, and split the sum above into two parts, with $\nu < 2\overline{\nu}$ and $\nu \geq 2\overline{\nu}$. We assume that ρ is already small, so that $\kappa \equiv \sqrt{2\overline{\nu}}\rho/l_z$ is a small parameter. In the $\nu < 2\overline{\nu}$ part of the sum, the Bessel function can be approximated by its asymptotic form

$$K_0(x \to 0) \sim -\log(x/2) - \gamma_E. \qquad (A1)$$

In the $\nu \geq 2\overline{\nu}$ part, on the other hand, K_0's argument is well approximated by $\sqrt{\nu}\rho/l_z$, and we can make use of the asymptotic form of the Hermite functions in the limit $\nu \to \infty$,

$$\frac{\phi_\nu^2(d_{\alpha\beta})}{\phi_0^2(0)} \sim \sqrt{\frac{2}{\pi}} \frac{\cos^2\left(\frac{d_{\alpha\beta}}{l_z}\sqrt{\nu + \frac{1}{2}} - \nu\frac{\pi}{2}\right)}{\sqrt{\nu}}.$$

As ν varies in this part of the sum, the $\cos^2$ term averages out to $1/2$, whereas K_0's argument changes only slowly, ρ/l_z being a small parameter. Thus, the $\nu \geq 2\overline{\nu}$ part of the sum in Eq. (A1) can be approximated by an integral,

$$\sum_{\nu=2\overline{\nu}}^\infty \frac{\phi_\nu^2(d_{\alpha\beta})}{\phi_0^2(0)} K_0\left(-iq_\nu\rho\right)$$

$$\simeq \sum_{\nu=2\overline{\nu}}^\infty \frac{1}{\sqrt{2\pi\nu}} K_0(\sqrt{\nu}\rho/l_z)$$

$$\simeq \frac{l_z}{\rho}\sqrt{\frac{2}{\pi}} \int_\kappa^\infty dx\, K_0(x)$$

$$\simeq \frac{l_z}{\rho}\sqrt{\frac{2}{\pi}} \left(\frac{\pi}{2} + \kappa\left(\log\frac{\kappa}{2} + \gamma_E - 1\right)\right),$$

with $x = \sqrt{\nu}\,\rho/l_z$, where we made use of the formula $\int_0^\infty K_0(x)\,dx = \pi/2$ and of the asymptotic form of K_0 in Eq. (A1). Finally, by putting the two parts of the sum together, we can take the limits $\rho \to 0$ and $\nu \to \infty$ (by keeping $\kappa \to 0$), and get

$$w_{\alpha\beta} = \lim_{\overline{\nu}\to\infty}\left[c_{\overline{\nu}} - \sum_{\nu=0}^{2\overline{\nu}-1}\frac{\phi_\nu^2(d_{\alpha\beta})}{\phi_0^2(0)}\log\left(\frac{\nu}{2}-\frac{\epsilon+i0^+}{\hbar\omega_z}\right)\right.$$
$$\left. + \left(\log(\rho/\sqrt{2}l_z)+\gamma_E\right)\left(4\sqrt{\frac{\overline{\nu}}{\pi}}-2\sum_{\nu=0}^{2\overline{\nu}-1}\frac{\phi_\nu^2(d_{\alpha\beta})}{\phi_0^2(0)}\right)\right],$$

with $c_\nu = 2\sqrt{\frac{\nu}{\pi}}\log\frac{\nu}{e^2}$. In the $\overline{\nu}\to\infty$ limit the term in the second row above disappears, and we get back the desired form of $w_{\alpha\beta}$, as given below Eq. (12) in the main text.

This series representation of $w_{\alpha\beta}$, however, has particularly poor $\sim \log\overline{\nu}/\sqrt{\overline{\nu}}$ convergence properties, and also oscillatory behavior in the $d_{\uparrow\downarrow}\neq 0$ case, that make it impractical for numerical evaluations. In the following, we thus provide an integral representation of this expression, which is more useful for numerical applications. Generalizing the calculations of Ref. 38, we first rewrite the terms in Eq. (A1) in an integral representation,

$$\frac{\sqrt{2\pi}l_z}{\rho} = \frac{1}{\sqrt{2}}\int_0^\infty\frac{d\tau}{\tau^{3/2}}e^{-\rho^2/(4l_z^2\tau)},$$

and

$$\frac{K_0(-iq_\nu\rho)}{2\pi} = -\frac{\hbar^2}{m}\int\frac{d^2k}{(2\pi)^2}\frac{e^{i\mathbf{k}\rho}}{\epsilon+i0^+ - \left(\frac{\hbar^2q^2}{m}+\hbar\nu\omega_z\right)}$$
$$= \int_0^\infty\frac{d\tau}{4\pi\tau}e^{\tau(\epsilon/\hbar\omega_z-\nu)}e^{-\frac{\rho^2}{4l_z^2\tau}},$$

that holds for all values of ν above the threshold $\nu > \epsilon/\hbar\omega_z$. Let us thus choose an arbitrary integer $\hat{\nu} > \epsilon/\hbar\omega_z$, and rewrite the terms $\nu > \hat{\nu}$ in Eq. (A1) in the above form, leading to

$$w_{\alpha\beta} = \lim_{\rho\to 0}\left\{2\sum_{\nu=0}^{\hat{\nu}}\frac{\phi_\nu^2(d_{\alpha\beta})}{\phi_0^2(0)}K_0(-iq_\nu\rho)\right.$$
$$+\int_0^\infty\frac{d\tau}{\tau}e^{-\rho^2/(4l_z^2\tau)}\left[-\frac{1}{\sqrt{2\tau}}\right.$$
$$\left.\left.+\sum_{\nu=\hat{\nu}+1}^\infty\frac{\phi_\nu^2(d_{\alpha\beta})}{\phi_0^2(0)}e^{\tau(\epsilon/\hbar\omega_z-\nu)}\right]\right\}.\qquad\text{(A2)}$$

The infinite sum above can be carried out exactly by making use of the formula for the real space density matrix of a harmonic oscillator [75],

$$\sum_{\nu=0}^\infty\frac{\phi_\nu^2(z)}{\phi_0^2(0)}e^{-\tau\nu} = \sqrt{\frac{e^\tau}{2\sinh\tau}}e^{-\tanh(\tau/2)z^2/2l_z^2}.$$

In order to take the $\rho\to 0$ limit, we expand the Bessel function, K_0, up to linear order in ρ, and rewrite its

log(ρ) singularity in an integral form,

$$K_0(-iq_\nu\rho) \sim \left[i\pi - \gamma_E - \log\left(\frac{\nu\hbar\omega_z-\epsilon-i0^+}{4\hbar\omega_z}\right)\right.$$
$$\left.+\int_0^\infty\frac{d\tau}{\tau}\Theta\left(\frac{1}{4}-\tau\right)e^{-\rho^2/(4l_z^2\tau)}\right]/2,$$

with the Heaviside function $\Theta(\tau)$ and Euler's constant $\gamma_E \approx 0.577$. Substituting these expressions into Eq. (A2), we can take the $\rho \to 0$ limit, and write $w_{\alpha\beta}$ in the form

$$w_{\alpha\beta} = -\sum_{\nu=0}^{\hat{\nu}}\frac{|\phi_\nu(d_{\alpha\beta})|^2}{|\phi_0(0)|^2}\left[\log\left(\frac{\nu\hbar\omega_z-\epsilon-i0^+}{4\hbar\omega_z}\right)+\gamma_E\right]$$
$$+\int_0^\infty\frac{d\tau}{\tau}\left[e^{-\frac{\tau\epsilon}{\hbar\omega_z}}\sqrt{\frac{e^\tau}{2\sinh\tau}}e^{-\tanh(\tau/2)d_{\alpha\beta}^2/2l_z^2}-\frac{1}{\sqrt{2\tau}}\right.$$
$$\left.+\sum_{\nu=0}^{\hat{\nu}}\frac{|\phi_\nu(d_{\alpha\beta})|^2}{|\phi_0(0)|^2}\left(\Theta\left(\frac{1}{4}-\tau\right)-e^{\tau(\epsilon/\hbar\omega_z-\nu)}\right)\right].$$

Despite its complexity at first glance, this formula provides a simple and fast numerical method for calculating $w_{\alpha\beta}$, and we have used it to evaluate the scattering amplitudes, $f_{\alpha\beta}^{\nu\nu'}$, to high numerical accuracy.

Appendix B: Shaking experiment

In order to separate the motional degrees of freedom parallel and perpendicular to the two-dimensional planes, we rewrite the many-body Hamiltonian in Eq. (17) in terms of the annihilation operators

$$a_{\alpha n}(\mathbf{q}) = \int d^2\rho\int dz\, e^{-i\mathbf{q}\vec{\rho}}\varphi(z-z_\alpha^0)\psi_\alpha(\mathbf{r}).$$

The normalization of these operators is given by their commutation relations $[a_{\alpha n}(\mathbf{q}),a_{\alpha'n'}^\dagger(\mathbf{q}')] = (2\pi)^2\delta_{\alpha\alpha'}\delta_{nn'}\delta^{(2)}(\mathbf{q}-\mathbf{q}')$. In this basis, the many-body Hamiltonian $H = H_{\rm kin} + H_{\rm int}$ can be written in the form

$$H_{\rm kin} = \sum_{\alpha=\uparrow,\downarrow}\sum_{n=0}^\infty\int\frac{d^2q}{(2\pi)^2}\xi_{\alpha n}(\mathbf{q})a_{\alpha n}^\dagger(\mathbf{q})a_{\alpha n}(\mathbf{q}),$$

$$H_{\rm int} = \sum_{\alpha,\beta=\uparrow,\downarrow}\sum_{\mathbf{n},\mathbf{n}'}\int\frac{d^2k}{(2\pi)^2}\frac{d^2k'}{(2\pi)^2}\frac{d^2q}{(2\pi)^2}\frac{t_{\alpha\beta}^{\mathbf{n}\mathbf{n}'}}{2}$$
$$a_{\alpha n_1}^\dagger(\mathbf{k}+\mathbf{q})a_{\beta n_2}^\dagger(\mathbf{k}'-\mathbf{q})a_{\beta n_2'}(\mathbf{k}')a_{\alpha n_1'}(\mathbf{k}),$$

where $\xi_{\alpha n}(\mathbf{q}) = \hbar^2q^2/2m + n\hbar\omega_z - \mu_\alpha$ stands for the single particle energies measured from the corresponding chemical potential μ_α, and $\mathbf{n} = (n_1,n_2)$ denotes the harmonic channels of the interacting particles. The interaction parameter $\mathbf{t}_{\alpha\beta}^{\mathbf{n}\mathbf{n}'}$ is the bare T-matrix (vertex) of

interactions, and it is given by

$$
\begin{aligned}
\mathbf{t}_{\alpha\beta}^{\mathbf{nn}'} &= g_{\alpha\beta} \int_{-\infty}^{\infty} dz_1 \, dz_2 \, \delta(z_1 - z_2 + d_{\alpha\beta}) \\
&\qquad \varphi_{n_1}^*(z_1) \varphi_{n_2}^*(z_2) \varphi_{n_2'}(z_2) \varphi_{n_1'}(z_1) \\
&= g_{\alpha\beta} \sum_{N\nu\nu'} C_{N\nu}^{\mathbf{n}*} C_{N\nu'}^{\mathbf{n}'} \, \phi_\nu^*(d_{\alpha\beta}) \phi_{\nu'}(d_{\alpha\beta}),
\end{aligned}
$$

where the Clebsch-Gordan coefficients $C_{N\nu}^{\mathbf{n}}$ denote the overlaps $C_{N\nu}^{\mathbf{n}} = \langle N\nu | \mathbf{n} \rangle$.

Assuming an equal coupling of the magnetic field gradient to the spin components $h_\uparrow = h_\downarrow = h_0$ in Eq. (18), shaking of the layers is described by the modulation Hamiltonian $\delta H_\alpha = -h_0 \cos(\omega t) \, \Xi_\alpha$, with $\Xi_\alpha = z_\alpha/l_z$ given in many-body form as

$$
\Xi_\alpha = \sum_{n=0}^{\infty} \int \frac{d^2 q}{(2\pi)^2} \sqrt{\frac{n+1}{2}} \left(a_{\alpha n+1}^\dagger(\mathbf{q}) \, a_{\alpha n}(\mathbf{q}) + \text{h.c.} \right).
$$

Thus, the shaking excites $n \leftrightarrow (n+1)$ transitions in both layers, amounting to $n = 0 \to 1$ transitions in case of a strongly confined dilute Bose gas. In linear response theory, the shaking susceptibility is given by the Kubo formula

$$
\chi_\alpha(t) = i\Theta(t) \langle [\Xi_\alpha(t), \Xi_\alpha(0)] \rangle,
$$

which is approximated by taking into account the bubble diagrams in Fig. 8(a) with dressed propagators, as we explained in the main text. The self-energy corrections to the propagator are due to the interaction of the propagating particles with the thermal gas through the many-body T-matrix.

In the the diagrammatic approach, incoming particles are specified by their frequency ω, momentum $\mathbf{q}$, layer index α, and their transverse channel n. The two particle T-matrix corresponds to the vertex function within the field theoretical approach, and in the vacuum it is proportional to the scattering amplitudes in Eq. (12) with the total energy of the incoming bosons replaced by the sum of their frequencies, $\Omega = \omega_1 + \omega_2$ (see Ref. 38). Both Ω and the total incoming momentum $\mathbf{Q} = \mathbf{q}_1 + \mathbf{q}_2$ are conserved within the 'ladder' diagram approximation of Fig. 8(c), unlike n_1 and n_2, which are not conserved. However, similar to the two particle problem [38], it is possible to sum up the whole ladder series by transforming to center of mass and relative coordinates and to the corresponding quantum numbers, $\{n_1, n_2\} \to \{N, \nu\}$. The total many-body vertex in Fig. 8(c) can then be expressed as

$$
\mathbf{T}_{\alpha\beta}^{\mathbf{n};\mathbf{n}'}(\Omega, \mathbf{Q}) = \sum_{N,N',\nu,\nu'} C_{N\nu}^{\mathbf{n}*} C_{N'\nu'}^{\mathbf{n}'} \, \mathbf{T}_{\alpha\beta}^{NN';\nu,\nu'}(\Omega, \mathbf{Q}),
$$

with the Clebsch-Gordan coefficients $C_{N\nu}^{\mathbf{n}}$ defined in Appendix B. In the strongly confined Bose gas, where only the lowest $n = 0$ level is populated, the T-matrix becomes diagonal in the center of mass index, $\mathbf{T}_{\alpha\beta}^{NN';\nu,\nu'} \to \delta_{NN'} \mathbf{T}_{\alpha\beta}^{N;\nu,\nu'}$, and is given by

$$
\mathbf{T}_{\alpha\beta}^{N;\nu,\nu'}(\Omega, \mathbf{Q}) = \frac{\hbar^2}{m} \frac{4\pi a_{\alpha\beta} \, \phi_\nu^*(d_{\alpha\beta}) \phi_{\nu'}(d_{\alpha\beta})}{1 + \frac{a_{\alpha\beta}}{\sqrt{2\pi} l_z} \mathcal{W}_{\alpha\beta}^N(\Omega, \mathbf{Q})},
$$

with the many-body counterpart $\mathcal{W}_{\alpha\beta}^N$ of $w_{\alpha\beta}$,

$$
\mathcal{W}_{\alpha\beta}^N(\Omega, \mathbf{Q}) = w_{\alpha\beta}\,(\epsilon/\hbar\omega_z) + \delta_{N0}\, \delta w_{\alpha\beta}^{\text{th}}(\Omega, \mathbf{Q}),
$$

with $\epsilon = \hbar\Omega - N\hbar\omega_z - \hbar^2 Q^2/4m$. The first term in $\mathcal{W}$ is just the vacuum contribution computed earlier, while the second term accounts for many-body interactions with other thermal bosons, and it is proportional to the density,

$$
\delta w_{\alpha\beta}^{\text{th}}(\Omega, \mathbf{Q}) = -\frac{4\pi}{m} \sqrt{2\pi} l_z \, |\phi_0(d_{\alpha\beta})|^2 \, \Pi_{\alpha\beta}^{\text{th}}(\Omega, \mathbf{Q}),
$$

with

$$
\Pi_{\alpha\beta}^{\text{th}}(\Omega, \mathbf{Q}) = \sum_{\gamma=\alpha,\beta} \int \frac{d^2 q}{(2\pi)^2} \frac{n_B\left(\frac{\hbar^2 (\frac{\mathbf{Q}}{2} + \mathbf{q})^2}{2m} - \mu_\gamma \right)}{\frac{\Omega + i0^+}{\hbar} - \frac{Q^2}{4m} - \frac{q^2}{m}},
$$

where n_B denotes the Bose distribution function. $\delta w_{\alpha\beta}^{\text{th}}$ describes the screening effect of the thermal gas. In case of a dilute Bose gas, however, its contribution to the dressed Green's functions turns out to be numerically small, and most features observed in the shaking experiment are dominated by the vacuum scattering amplitudes, determined by just $w_{\alpha\beta}$. Neglecting thermal corrections, the T-matrix becomes proportional to the vacuum scattering amplitudes

$$
T_{\alpha\beta}^{N;\nu\nu'}(\Omega, \mathbf{Q}) \approx \frac{\hbar^2}{m} f_{\alpha\beta}^{\nu\nu'} \left(\hbar\Omega - N\hbar\omega_z - \frac{\hbar^2 Q^2}{4m} \right).
$$

In calculating the self-energy, $\Sigma_\alpha^{nn'}$, due to the diluteness of the gas, we only keep terms proportional to the square of the density, leading to

$$
\begin{aligned}
\Sigma_\alpha^{nn'}(\omega, \mathbf{q}) &\approx \sum_{\beta=\uparrow,\downarrow} \sum_{\tilde{n}=0}^{\infty} \int \frac{d^2 k}{(2\pi)^2} \, n_B \left(\frac{\hbar^2 \mathbf{k}^2}{2m} + \tilde{n}\hbar\omega_z - \mu_\beta \right) \\
&\quad \mathbf{T}_{\alpha\beta}^{n\tilde{n}, n'\tilde{n}} \left(\omega + \frac{\hbar k^2}{2m} + \tilde{n}\omega_z, \mathbf{k} + \mathbf{q} \right).
\end{aligned}
$$

Having the self-energies at hand, we can proceed and compute the spectral functions of the Green's functions, $\rho_\alpha^{nn'}(\omega, \mathbf{q}) = -\text{Im}(G_R)_\alpha^{nn'}(\omega, \mathbf{q})/\pi$. In terms of the spectral functions, the shaking susceptibility takes on a particularly simple form. In the strongly confined gas only the lowest $n = 0, 1$ levels give dominant contributions to the susceptibility, thus we obtain

$$
\begin{aligned}
\chi_\alpha(\omega) &= \int \frac{d\tilde{\omega}}{2} \frac{d^2 \tilde{q}}{(2\pi)^2} \, n_B(\tilde{\omega} - \mu_\alpha) \left[\rho_\alpha^{00}(\tilde{\omega}, \tilde{q}) \rho_\alpha^{11}(\tilde{\omega} + \omega, \tilde{q}) \right. \\
&\quad \left. + 2 \rho_\alpha^{01}(\tilde{\omega}, \tilde{q}) \, \rho_\alpha^{01}(\tilde{\omega} + \omega, \tilde{q}) + \{\omega \leftrightarrow -\omega\} \right].
\end{aligned}
$$

We determine the above integrals numerically, and arrive at the shaking spectrum $\dot{\epsilon}(\omega) = \sum_\alpha h_\alpha^2 \, \omega \chi_\alpha''(\omega)/2$, shown in Fig. 9.

—

[1] C. Nayak, S. H. Simon, A. Stern, M. Freedman, and S. Das Sarma, Rev. Mod. Phys. **80**, 1083 (2008).
[2] F. D. M. Haldane, Phys. Rev. Lett. **61**, 2015 (1988).
[3] B. A. Bernevig, T. L. Hughes, and S.-C. Zhang, Science **314**, 1757 (2006).
[4] P. A. Lee, N. Nagaosa, and X.-G. Wen, Rev. Mod. Phys. **78**, 17 (2006).
[5] Z. Hadzibabic, P. Krüger, M. Cheneau, B. Battelier and J. Dalibard, Nature **441**, 1118 (2006).
[6] E. Haller *et al.*, Science **325**, 1224 (2009).
[7] A. Görlitz *et al.*, Phys. Rev. Lett. **87**, 130402 (2001).
[8] E. Haller *et al.*, Phys. Rev. Lett. **104**, 153203 (2010).
[9] N. L. Smith, W. H. Heathcote, G. Hechenblaikner, E. Nugent, and C. J. Foot, J. Phys. B: At. Mol. Opt. Phys. **38**, 223 (2005).
[10] C.-L. Hung, X. Zhang, N. Gemelke, and C. Chin, Nature **470**, 236 (2011).
[11] P. Krüger, Z. Hadzibabic, and J. Dalibard, Phys. Rev. Lett. **99**, 040402 (2007).
[12] P. Cladé, C. Ryu, A. Ramanathan, K. Helmerson, and W. D. Phillips, Phys. Rev. Lett. **102**, 170401 (2009).
[13] M. Holzmann and W. Krauth, Phys. Rev. Lett. **100**, 190402 (2008).
[14] R. P. Feynman, Int. J. Theor. Phys. **21**, 467488 (1982).
[15] K. Van Houcke *et al.*, Nat. Phys. **8**, 366 (2012).
[16] L. V. Butov, A. C. Gossard, and D. S. Chemla, Nature **418**, 751 (2002).
[17] J. A. Seamons, C. P. Morath, J. L. Reno, and M. P. Lilly, Phys. Rev. Lett. **102**, 026804 (2009).
[18] E. Tutuc, M. Shayegan, and D. A. Huse, Phys. Rev. Lett. **93**, 036802 (2004).
[19] M. Kellogg, J. P. Eisenstein, L. N. Pfeiffer, and K. W. West, Phys. Rev. Lett. **93**, 036801 (2004).
[20] J. P. Eisenstein and A. H. MacDonald, Nature **432**, 691 (2004).
[21] Y. W. Suen, L. W. Engel, M. B. Santos, M. Shayegan, and D. C. Tsui, Phys. Rev. Lett. **68**, 1379 (1992).
[22] J. P. Eisenstein, G. S. Boebinger, L. N. Pfeiffer, K. W. West, and S. He, Phys. Rev. Lett. **68**, 1383 (1992).
[23] D. R. Luhman, W. Pan, D. C. Tsui, L. N. Pfeiffer, K. W. Baldwin, and K. W. West Phys. Rev. Lett. **101**, 266804 (2008)
[24] W. Bao *et al.*, Phys. Rev. Lett. **105**, 246601 (2010).
[25] B. E. Feldman, J. Martin, and A. Yacobi, Nat. Phys. **5**, 889 (2009).
[26] R. T. Weitz, M. T. Allen, B. E. Feldman, J. Martin, and A. Yacoby, Science **330**, 812 (2010).
[27] A. S. Mayorov *et al.*, Science **333**, 860 (2011).
[28] J. Velasco Jr. *et al.*, Nat. Nanotech. **7**, 156 (2012).
[29] M. W. Zwierlein, A. Schirotzek, C. H. Schunck, and W. Ketterle, Science **311**, 492 (2006).
[30] J. W. Park, C.-H. Wu, I. Santiago, T. G. Tiecke, S. Will, P. Ahmadi, and M. W. Zwierlein, Phys. Rev. A **85**, 051602(R) (2012).
[31] M. W. Zwierlein, J. R. Abo-Shaeer, A. Schirotzek, C. H. Schunck, and W. Ketterle, Nature **435**, 1047 (2005).
[32] P. Makotyn, C. E. Klauss, D. L. Goldberger, E. A. Cornell, and D. S. Jin, Nat. Phys. **10**, 116 (2014).
[33] S. Mukerjee, C. Xu, and J. E. Moore, Phys. Rev. Lett. **97**, 120406 (2006).
[34] D. Podolsky, S. Chandrasekharan, and A. Vishwanath, Phys. Rev. B **80**, 214513 (2009).
[35] M. Olshanii, Phys. Rev. Lett. **81**, 938 (1998).
[36] D. S. Petrov, M. Holzmann, and G. V. Shlyapnikov, Phys. Rev. Lett. **84**, 2551 (2000).
[37] D. S. Petrov and G. V. Shlyapnikov, Phys. Rev. A **64**, 012706 (2001).
[38] For the inclusion of many-body effects see V. Pietilä, D. Pekker, Y. Nishida, and E. Demler, Phys. Rev. A **85**, 023621 (2012).
[39] I. Bloch, J. Dalibard, W. Zwerger, Rev. Mod. Phys. **80**, 885 (2008).
[40] L. D. Landau and E. M. Lifshitz, *Quantum Mechanics: Non-Relativistic Theory* (Pergamon Press, New York, 1987).
[41] D. Pekker, M. Babadi, R. Sensarma, N. Zinner, L. Pollet, M. W. Zwierlein, and E. Demler, Phys. Rev. Lett. **106**, 050402 (2011).
[42] S. Sala *et al.*, Phys. Rev. Lett. **110**, 203202 (2013).
[43] B. Fröhlich, M. Feld, E. Vogt, M. Koschorreck, W. Zwerger, and M. Köhl, Phys. Rev. Lett. **106**, 105301 (2011).
[44] A. T. Sommer, L. W. Cheuk, M. J. H. Ku, W. S. Bakr, and M. W. Zwierlein, Phys. Rev. Lett. **108**, 045302 (2012).
[45] H. Moritz, T. Stöferle, K. Günter, M. Köhl, and T. Esslinger, Phys. Rev. Lett. **94**, 210401 (2005).
[46] P. J. Lee, M. Anderlini, B. L. Brown, J. Sebby-Strabley, W. D. Phillips, and J. V. Porto, Phys. Rev. Lett. **99**, 020402 (2007).
[47] O. Mandel, M. Greiner, A. Widera, T. Rom, T. W. Hänsch, and I. Bloch, Phys. Rev. Lett. **91**, 010407 (2003).
[48] P. Soltan-Panahi *et al.*, Nat. Phys. **7**, 434 (2011).
[49] In particular, we use the pseudopotential $V_{\alpha\beta}(\mathbf{r})\,(\dots) = \left(4\pi\hbar^2 a_{\alpha\beta}/m\right)\delta(\mathbf{r})\frac{\partial}{\partial_r}\left(r\dots\right)$ which is a good approximation whenever the trapping potential is approximately constant within the effective range of interactions, R_e [37, 39]. Then, R_e is required to be small compared to the oscillator length, $l_z \equiv \sqrt{\hbar/(m\omega_z)}$, and layer separations are also restricted to the range $d_{\uparrow\downarrow} \ll l_z^2/R_e$. Since $R_e \sim 1-10\,$nm for most atoms [37, 76], these conditions are very well satisfied in standard experiments. For the case of extremely strong trapping frequencies, where $l_z \sim R_e$, see Refs. 77 and 78.
[50] Throughout this paper, we refer to the scattering states of resonant scattering amplitudes as quasi-bound molecular states. The width of these resonances are identified as the inverse lifetime of the quasi-bound state.
[51] P. Wicke, S. Whitlock, and N. J. van Druten, arXiv:1010.4545.
[52] T. Kinoshita, T. Wenger, and D. S. Weiss, Science **305**, 1125 (2004).
[53] B. Paredes *et al.*, Nature **429**, 277 (2004).
[54] W. Fu, Z. Yu and X. Cui, Phys. Rev. A **85**, 012703 (2012).
[55] Although many-body effects are different for and fermionic gases, the two-particle scattering properties, discussed in this Section are the same for bosons and fermions with the modification that fermionic atoms are non-interacting in the s-wave channel [39], implying

$a_{\uparrow\uparrow} = a_{\downarrow\downarrow} = 0$.

[56] For notational simplicity, we omit the indices $\alpha\beta$ of $\mathcal{H}_{\mathrm{rel}}$ throughout the paper.

[57] The relative wave function Ψ_{rel} must be symmetrical for bosons, and antisymmetrical for fermions.

[58] Throughout this paper we assume that a set of real harmonic oscillator wave functions is used.

[59] In case of identical bosons, $\alpha = \beta$, the right hand side of Eq. (4) contains an extra factor of two [37].

[60] A. Messiah, *Quantum Mechanics, Volume II* (Elsevier Science B. V., 1961).

[61] This wave function is essentially exact at separations larger than the range of atom-atom interaction.

[62] We speculate that these bound states, shifted to positive energies, may create Feshbach resonances in the interaction both in interlayer and in interlayer scattering, if some kind of anharmonicity resonantly couples the relative and center of mass motion of particles. Such a coupling may arise from a difference between the trapping frequencies of the two layers (e.g. in case of bosonic mixtures), or from anharmonicities of the trapping potential [42].

[63] For standard trapping frequencies $\omega_z/(2\pi) = 1-100\,\mathrm{kHz}$, depending also on the atomic species used in the experiment, our approximations are valid up to rather large layer separations, $d_{\uparrow\downarrow}/l_z \sim 3-10$ [49].

[64] Indeed, the excited states transformed into the basis of center of mass and relative coordinates are given by $|n_\alpha = 1, n_\beta = 0\rangle = (|N = 1, \nu = 0\rangle + |N = 0, \nu = 1\rangle)/\sqrt{2}$.

[65] Notice that Fig. 5 displays only the relative motion's energy, and to obtain the total energy, one should add the center of mass motion's energy, $N\hbar\omega_z + Q^2/4m$.

[66] Although in case of extreme trapping frequencies, $\omega_z/2\pi \gg 100$ kHz, the pseudopotential, describing the pair interactions between the particles, may require energy dependent corrections [77, 78], we expect the overall scattering behavior in the confined system to be only slightly modified by these terms.

[67] The magnetic field gradients required in this case to reach a separation $d_{\uparrow\downarrow} \sim l_z$ are rather small, $\nabla B_z \sim$ 0.01 − 1 G/mm, they nevertheless lead to a weak magnetic field difference between the centers of the layers, in the range of $\Delta B \sim 10 - 100$ mG. In case of very narrow Feshbach resonances whose width are comparable to ΔB, this can result in a spatially varying value of the scattering lengths, making our results inapplicable in this case.

[68] A. Widera *et al.*, Phys. Rev. Lett. **100**, 140401 (2008).

[69] C. Chin, R. Grimm, P. Julienne, and E. Tiesinga, Rev. Mod. Phys. **82**, 1225 (2010).

[70] G. Modugno, M. Modugno, F. Riboli, G. Roati, and M. Inguscio, Phys. Rev. Lett. **89**, 190404 (2002).

[71] G. Thalhammer, G. Barontini, L. De Sarlo, J. Catani, F. Minardi, and M. Inguscio, Phys. Rev. Lett. **100**, 210402 (2008).

[72] J. Catani, L. De Sarlo, G. Barontini, F. Minardi, and M. Inguscio, Phys. Rev. A **77**, 011603(R) (2008).

[73] S. B. Papp, J. M. Pino, and C. E. Wieman , Phys. Rev. Lett. **101**, 040402 (2008).

[74] The results of this paper can be carried through to bosonic mixtures with different masses, $m_\uparrow$ and $m_\downarrow$, but trapped with equal trapping frequencies, ω_z. By introducing the center of mass, $M_{\alpha\beta} = m_\alpha + m_\beta$, the reduced mass, $\mu_{\alpha\beta}^r = \frac{m_\alpha m_\beta}{m_\alpha + m_\beta}$, and the oscillator length, $l_{\alpha\beta}^z = \sqrt{\hbar/(2\mu_{\alpha\beta}^r \omega_z)}$, in channels $\alpha\beta$, our results can be simply rewritten by appropriately substituting these values for the center of mass $2m \to M_{\alpha\beta}$, the reduced mass $m/2 \to \mu_{\alpha\beta}^r$ and the oscillator length $l_z \to l_{\alpha\beta}^z$.

[75] R. P. Feynman, *Statistical Mechanics: A Set Of Lectures* (Westview Press, 1998).

[76] Y. Castin in *'Coherent atomic matter waves'*, *Lecture Notes of Les Houches Summer School*, edited by R. Kaiser, C. Westbrook, and F. David (EDP Sciences and Springer-Verlag, 2001).

[77] D. Blume and C. H. Greene, Phys. Rev. A **65**, 043613 (2002).

[78] P. Naidon, E. Tiesinga, W. F. Mitchell and P. S. Julienne, New. J. Phys. **9**, 19 (2007).